CLM - P 364

UKAEA RESEARCH GROUP

Preprint

AN EXPERIMENTAL INVESTIGATION OF PARALLEL AND OBLIQUE SHOCK WAVES IN A MAGNETIZED PLASMA

A D CRAIG

CULHAM LABORATORY
Abingdon Berkshire

1973

CLM - P 364

AN EXPERIMENTAL INVESTIGATION OF PARALLEL AND OBLIQUE SHOCK WAVES IN A MAGNETIZED PLASMA

by

A.D. CRAIG

(Submitted for publication in J. Plasma Phys.)

ABSTRACT

The CHARYBDIS apparatus is designed to produce parallel and oblique shock waves in a magnetized plasma.

An initial hydrogen plasma ($n_{el} \sim 7 \times 10^{20}$ m^{-3}, $T_1 \sim 1.3$ eV) is produced in a pyrex chamber (0.46 m diameter, 1.25 m long) containing an axial magnetic field (B_{z1} up to 0.2 T). A magnetic piston is produced by a fast rising radial discharge between a central electrode and an annular outer electrode at one end of the chamber. The Lorentz force on the current sheet causes axial motion and a quasi-steady shock profile propagates ahead. A clear shock-piston separation is achieved across almost the complete radial extent for a wide range of initial parameters. The shock propagation angle to the initial field ranges from 0° to 40°.

The Alfven Mach number (M_A) of the flow is varied by changing the initial field strength. Switch-on shock behaviour is demonstrated at a point of parallel propagation for low M_A. For higher M_A cases no separated point of parallel propagation occurs in the shock profile.

U K A E A Research Group,
Culham Laboratory,
Abingdon,
Berks.

September, 1973

1. INTRODUCTION

This paper describes an experimental investigation of parallel and oblique shock waves in a magnetized hydrogen plasma. In particular it extends an earlier investigation (Craig and Paul, 1973, hereafter referred to as Paper I) concerned with the possible existence of 'switch-on' shock waves.

1.1 Properties of Parallel and Oblique Hydromagnetic Shock Waves

A review of the theory and properties of parallel hydromagnetic shock waves has been given in Paper I. Only the salient points will be repeated here.

A purely gasdynamic, i.e. non-magnetic, solution to the conservation relations exists for the case of a shock wave propagating into a magnetized plasma in a direction parallel to the field. For high Alfven Mach numbers (M_A) this gasdynamic solution is stable according to the usual criterion that the plasma flow velocity, in a frame of reference moving with the shock, crosses only one linear wave speed within the shock (Anderson, 1963). In this case only the fast wave speed is crossed ($v_1 > c_{f1}$; $c_{s2} = c_{i2} < v_2 < c_{f2}$) where the suffices 1 and 2 refer to pre-shock and post-shock conditions and c_f, c_i and c_s are the fast, intermediate and slow linear wave speeds.

As M_A is decreased however, a critical value is reached ($\hat{M}_A$) below which the gasdynamic solution involves a velocity transition which crosses c_i and c_s in addition to c_f. Such a solution is therefore not stable. In the Mach number regime $1 < M_A < \hat{M}_A$ there does however exist a second solution to the conservation equations which involves the production of transverse components of velocity and magnetic field behind the shock; this is the so-called 'switch-on' shock. A property of the 'switch-on' shock solution that has aroused much theoretical interest is that $v_2 = c_{i2}$ and consequently the stability is marginal.

The value of $\hat{M}_A$ varies with the preshock parameter $\beta_1 (= 4\mu_o n k T_1 / B_1^2)$ according to

$$\hat{M}_A = \left(\frac{\gamma + 1 - \gamma\beta_1}{\gamma - 1} \right)^{\frac{1}{2}}$$

i.e. $\hat{M}_A$ decreases with β_1 from $\hat{M}_A = [(\gamma+1)/(\gamma-1)]^{\frac{1}{2}}$ ($= 2$ for $\gamma = 5/3$) for $\beta_1 = 0$ to $\hat{M}_A = 1$ for $\beta_1 = 2/\gamma$. Thus for $\beta_1 \geq 2/\gamma$ no switch-on shock solutions exist. The magnitude of the 'switched-on' transverse field is given by

$$\frac{B_{T2}}{B_1} = \left\{ \left(M_A^2 - 1 \right) \left[\gamma + 1 - \gamma\beta_1 - M_A^2 (\gamma - 1) \right] \right\}^{\frac{1}{2}} .$$

This function is plotted in Paper I for the case $\beta_1 = 0$.

It is clear that the direction of the 'switched-on' field and velocity components is undefined. However if

the shock propagation direction, i.e. the shock normal, is at all oblique to the preshock field, then a direction is defined for the post-shock transverse field and velocity components; they must remain in the plane defined by the propagation direction and the pre-shock field (Kantrowitz and Petschek, 1966).

1.2 Previous Experiments

We present a brief review of previous experiments concerned with the production of oblique and parallel shocks in a magnetized plasma.

In an experiment described by Robson and Sheffield (1968) a fast rising current in a short theta pinch type coil around a large diameter discharge tube drives an imploding curved magnetic piston into a low β magnetized plasma. A curved shock profile propagating at angles to the initial field ranging from 90° at the midplane to 40° at the ends is produced ahead of the piston. Alfven Mach numbers are up to $M_A = 5$. In the oblique region the shock structure is characterised by precursor whistler oscillations; the wavelength is shown to vary with shock angle and M_A in accordance with the theoretical dispersion relation. Comparison of experimental shock structures with theoretical structures based on a two-fluid hydromagnetic model demonstrates the presence of a collisionless dissipation mechanism; the ion-sound instability is

suggested as this mechanism. A later report on this same device (Sheffield et al., 1970) describes laser light scattering measurements of the electron temperature transition through the shock wave. For M_A less than the critical Mach number (M_A^*) the heating goes predominantly to the electrons whilst, for higher M_A values, there is evidence that the ion heating increases.

Attempts to produce parallel hydromagnetic shocks in the switch-on regime have been made by Watson-Munro et al. (1968) and Kurtmullaev et al (1971) using annular shock tube and conical theta pinch gun respectively. In neither case is parallel propagation or shock-piston separation clearly demonstrated.

Paper I (Craig and Paul, 1973) describes results from a large annular shock tube. A radial discharge initiated between a short centre electrode and an annular electrode at one end of the discharge chamber moves axially under the $\underline{J}_r \times \underline{B}_\theta$ force into an initial plasma containing an axial magnetic field. A central plasma pinch developing out of the short centre electrode feeds current to the propagating front and the return current flows in plasma adjacent to the outer wall. For a limited range of conditions the propagating discharge successfully acts as a magnetic piston and, for a limited radial extent ($25 < r < 75$ mm), a clearly separated curved shock profile propagates

ahead. The profile includes a point of parallel propagation where switch-on shock behaviour, with post-shock B_θ and v_θ components, is demonstrated to be in agreement with conservation theory for the measured M_A. Away from the point of parallel propagation, where the shock is oblique, the requirement that the post-shock field remains in the rz plane is not satisfied; $\dot{B}_\theta$ is the dominant post-shock field. A model is suggested in which a large amplitude intermediate wave, propagating behind the oblique shock, rotates the post-shock field and velocity components. Although the experimental production of a stable switch-on shock is demonstrated the situation is somewhat unsatisfactory for the following reasons:

(i) Radial plasma motion occurs within and behind the shock profile due to centrifugal effects of the v_θ velocity.

(ii) The comparatively small radius of curvature of the shock profile makes the validity of comparison with one dimensional conservation relations somewhat uncertain.

(iii) Reproducibility is not good due to instability in the central pinch.

2. CHARYBDIS APPARATUS

In an attempt to improve the reproducibility of the flow, the short centre electrode of the apparatus of

Paper I was replaced by a long centre electrode ($\ell = 0.9$ m, dia. = 57 mm). This modification not only improved the reproducibility but also the basic flow pattern in that a better shock separation over a larger radial extent was obtained; it is this new flow pattern which forms the subject of the present paper.

The apparatus is shown schematically in Fig.1. The main vacuum vessel consists of a pyrex glass cylinder (1.25 m long, 0.46 m dia) with stainless steel end plates. Hydrogen was used in all the experiments discussed in this paper with filling pressures typically 20 - 40 mtorr.

A slow rising axial magnetic field (B_{z1}) of up to 0.2 Tesla is produced by discharging a capacitor bank through a set of six coils. The current is clamped at its peak and the field remains essentially constant throughout the period of the discharge. The field is uniform to within 2 percent throughout the main volume of the discharge chamber, i.e. from the launch end, at $z = 0$ to $z = 0.9$ m.

An initial plasma is produced by an oscillatory axial current (100 μsec period, 110 kA peak) between the annular electrode at the launch end and the far end plate. The current damps over five half cycles and is zero for $t > 250$ μsec.

The main radial discharge is produced by applying a potential at 40 kV between the stainless steel centre electrode (ℓ = 0.9 m, dia = 57 mm, negative polarity) and the outer annular electrode used for the preheating discharge. The capacitor bank is in halves feeding opposite sides of the apparatus through transmission lines. A two stage pulse shaping circuit gives a first approximation to a square wave with the current rising in 0.5 μsec to a peak I_p = 180 kA and remaining approximately constant for 3 μsec. The radial current sheet moves axially under the $\underline{J}_r \times \underline{B}_\theta$ force and rotates under the $\underline{J}_r \times \underline{B}_z$ force.

3. INITIAL PLASMA

A full description of the measurement of the initial plasma parameters, $n_e(r,z,t)$ and $T_e(r,z,t)$, in CHARYBDIS has been given in Paper I. The density and temperature distributions were made using a double Langmuir probe and an absolute density calibration was made using a He-Ne laser interferometer.

With the long centre electrode in place the only modification to the previous distributions was in the presence of a 50 mm thick sheath of neutral atoms around the centre electrode. Fig.2 shows the radial distribution of n_e at $z = 0.46$ m for the case, $B_{z1} = 0.2$ T and $p = 40$ mtorr at the time of initiation of the radial discharge, i.e.

$t = 300\ \mu sec$ after the start of the preheat discharge. A region of uniform density exists for $70 < r < 180$ mm. The electron temperature is $\sim 1.5 \times 10^4$ K and is independent of position.

No direct measurement of the neutral atom density $n_n(r,z,t)$ was made but as in Paper I we draw on the similarity between the CHARYBDIS initial plasma and that of the TARANTULA experiment for which measurements (Paul, 1970) show $n_n \approx 0.1\, n_e$. The neutral density is involved because, for frequencies below ~ 1 MHz, such as occur in the main flow, the neutrals are coupled into the plasma by charge exchange collisions.

4. EXPERIMENTAL OBSERVATIONS : PISTON AND OBLIQUE SHOCK

This section describes the detailed flow dynamics for one set of initial conditions, $B_{z1} = 0.2$ T and $p = 20$ mtorr (H_2). A similar flow was observed, however, over a wide range of initial conditions.

4.1 Current Flow in the rz Plane

The radial variation of B_θ was measured at a series of axial positions (0.1 m intervals). Fig.3 shows a typical $B_\theta(r)$ distribution behind the main current front. The dashed curve is a r^{-1} distribution normalised at $r = 50$ mm, i.e. the distribution that would result if all the current feeding the propagating front flowed within

the centre electrode. It is clear that some axial current is present across the complete radial extent. The small standard deviation error bars represent a considerable improvement in reproducibility compared with an equivalent distribution using the short centre electrode configuration (Paper I).

A series of measured $B_\theta(r,t)$ distributions were analysed to produce the current contours of Fig.4; the currents indicated are enclosed radially within the contours.

At $t = 2\,\mu$sec (Fig.4(a)) the total applied current is at its peak. About 80 kA flows in a tilted, high current density front whilst the remainder is distributed in the region behind the front.

At $t = 4\,\mu$sec (Fig.4(b)) the total applied current has dropped to zero, i.e. none of the contours can terminate at the electrodes. The decrease of the applied current has no immediate effect on the main propagating current front.

4.2 Identification of the Shock Wave

Fig.5(a) shows a set of typical magnetic field oscillograms (δB_z, B_r and B_θ at $r = 142.5$ mm, $z = 0.4$ m) taken simultaneously with an axially inserted multiple magnetic probe having three coils of 20 turns and 1.5 mm diameter enclosed in a pyrex glass shield of 5 mm outside diameter. We note

(i) All three components display precursor oscillations.

(ii) A field rise in B_r and B_z occurs at the end of the oscillations whereas B_θ returns to zero.

(iii) A rise in B_θ follows $\sim 0.7\,\mu$sec after the B_r rise whilst B_r and B_z decrease. This rise in B_θ is the propagating current front discussed in the section 4.1.

(iv) Within the precursor oscillations, shown on a higher amplication in Fig.5(b) and (c), the B_r and δB_z components are in phase (the slight apparent phase difference on the oscillogram is due to a 4 mm axial separation of B_r and B_z sensing coils) and the B_r and B_θ components are 90° out of phase.

Clearly this structure is an oblique shock wave (rise in B_r and B_z) followed by and separated from its driving piston (rise in B_θ and changes in B_r and B_z arising from diamagnetic and rotational effects). The precursor oscillations are the whistler oscillations characteristic of the structure of dispersive oblique and parallel hydromagnetic shocks. This model is illustrated in Fig.5(d) The effective shock velocity is $V_s \cos\alpha$ where V_s is the velocity of the shock in the axial direction and α is the tilt angle. Behind the shock we have

$$B_{y2} > B_{y1} \quad , \quad B_{x2} = B_{x1}$$

or in the cylindrical notation

$$B_{r2} > 0 , \quad B_{z2} > B_{z1} , \quad B_{\theta 2} = 0 .$$

The changes in B_z and B_r across the shock may be expressed as

$$\delta B_z = (B_{y2} - B_{y1}) \sin \alpha$$
$$\delta B_r = (B_{y2} - B_{y1}) \cos \alpha .$$

It follows that

$$\tan \alpha = \frac{\delta B_z}{\delta B_r}$$

and thus the shock angle can be determined from the experimentally measured ratio of changes in B_z and B_r across the shock. The shock of Fig.5 therefore has a tilt angle $\alpha \sim 20^\circ$.

4.3 Precursor Whistler

Whistler waves are characterised by a rotation of the magnetic field component transverse to the propagation direction. The tilt angle of the propagation can therefore again be obtained from $\tan^{-1}(\delta B_z/\delta B_r)$. Analysis of Fig.5(b) and (c) shows the propagation direction to be $\sim 20^\circ$ from axial, i.e. in the same direction as the main shock front. Fig.6 shows the rotation of the transverse field in the plane of the shock for the case of Fig.5.

By comparing the measured whistler wavelength at the front of the shock, i.e. before the initial plasma para-

meters are appreciably modified, with the theoretical wavelength (Stringer, (1963))

$$\lambda = \frac{2\pi M_A \cos\alpha}{(M_A^2 - 1)^{\frac{1}{2}} (M_A^2 - \cos^2\alpha)^{\frac{1}{2}}} \left(\frac{c}{\omega_{pi}}\right)$$

we may make a further check on the density (n_i) of the initial plasma. The measured wavelength of $\lambda = 54$ mm requires a preheat density of $n_i = 6.5 \times 10^{20}$ m^{-3} to be compared with the directly measured value of $\sim 6 \times 10^{20}$ m^{-3} (NB. Fig.2 is for 40 mtorr filling pressure.)

4.4 Axial Propagation

The axial propagation of the shock and piston is illustrated in Figs.7 and 8. The oscillograms show the shock structure to remain approximately steady but some steepening of the piston is apparent with dispersive structure appearing at $z = 0.6$ m. The $z(t)$ plot shows the shock (peak $\dot{B}_r$) and piston (peak $\dot{B}_\theta$) velocities to be approximately constant over a large axial range and the shock-piston separation is clearly seen to increase with z. Typical shock and piston velocities are 2.8×10^5 and 2.0×10^5 m/sec respectively.

4.5 Shock Profile

The shape of the shock profile was determined from the radial variation of its arrival time at a given axial position. Fig.4(a) shows the shock piston at $t = 2$ μsec.

A clear shock-piston separation (up to 120 mm) is present over a large radial extent. The separation decreases at lower radii and, with finite structure thickness, there is some overlapping.

Fig.9 shows the radial variation in arrival time of the shock at a series of axial positions. It is seen that the general shape of the shock profile remains steady. There does however appear to be some fine structure on the profiles which is not merely the result of shot-to-shot irreproducibility. The feature marked 'A' propagates along the shock with a velocity of $\sim 4 \times 10^4$ m/sec. This fine structure is smoothed out in the shock profile of Fig.4(a).

The axial variation of tilt angle α at $r = 142.5$ mm, as measured from the ratio of B_z and B_r field transitions, is illustrated in Fig.10. The approximately constant tilt between $z = 0.2$ and 0.7 m again shows the quasi-steady profile.

4.6 Discussion

A shock-piston situation has been produced in an annular geometry with

(i) A quasi-steady shock profile propagating over a large axial distance into a well diagnosed initial plasma.

(ii) A clear shock-piston separation over a large radial extent.

(iii) A large radius of curvature on the shock profile such that comparison with one dimensional theory is reasonable.

(iv) No v_θ component between the shock and piston producing complicating centrifugal effects.

(v) A high degree of reproducibility.

This is an improvement over the situation described in Paper I and allows the following detailed shock studies to be made.

5. EXPERIMENTAL OBSERVATIONS : DETAILED SHOCK MEASUREMENTS

We consider detailed shock wave measurements for the three sets of parameters listed in Table I. In cases (1) and (2) $M_A < \hat{M}_A$ for $\alpha = 0$ and thus the parallel shock should be of the switch-on type. In case (3) the parallel shock should be of the gasdynamic type.

TABLE I

Case	(1)	(2)	(3)
B_{z1} (T)	0.20	0.15	0.10
p_1 (mtorr)	40	40	40
$n_{el_{Ave.}}$ ($\times 10^{20}$ m^{-3})	$\sim$ 5.5 (4.7 at r = 70 mm)	$\sim$ 5.5	$\sim$ 5.5
$T_{el_{Ave.}}$ ($\times 10^4$ K)	$\sim$ 1.5	$\sim$ 1.5	$\sim$ 1.5
β_1	0.014	0.025	0.056
$\hat{M}_A$	1.995	1.985	1.965
V_s ($\times 10^5$ m/sec)	2.4	2.4	2.2
v_A ($\times 10^5$ m/sec)	1.87 (2.00 at r = 70 mm)	1.40	0.93
$M_A(\alpha = 0)$	1.2	1.72	2.36

5.1 Case (1): Low M_A Switch-on Shock

Fig.11(a) shows the radial variation of shock and piston arrival times at $z = 0.4$ m. We note

(i) a separated point of parallel propagation exists in the shock profile at $r^* \sim 70$ mm; at this point $M_A \sim 1.2$ and hence the shock should be of the switch-on type;

(ii) the profile appears to pass smoothly through this point of parallel propagation with a negative tilt angle α in the region $r < r^*$.

(iii) there is a discontinuity in the profile at $r \sim 150$ mm; this is probably a wave propagating along the front as in Fig.9.

The experimentally measured magnetic field transition across the shock can be compared with the theoretical value from the conservation relations for the measured initial parameters, shock velocity and shock angle. It is convenient to consider the B_{r2} component only. Fig.11(b) shows the experimental $B_{r2}(r)$ distribution corresponding to the profile of Fig.11(a) and the theoretical $B_{r2}(r)$ distribution, calculated from the conservation relations, for the best-fit experimental profile of Fig.11(a) and the $n_{el}(r)$ distribution of Fig.2 (with neutrals $n_{nl} = 0.1\ n_{el}$ also coupled). The agreement is good except for $r > 170$ mm; the decrease in the theoretical distributions is a result of the decrease in n_{el} at $r \sim 170$ mm. It is clear however that where the $n_{el}(r)$ distribution of the initial plasma shows a decrease at the boundaries the neutral atom density must increase to maintain a radial pressure balance, i.e. $n_n > 0.1\ n_e$ for $r > 170$ mm produces the high experimental B_{r2} values in this region.

It should be noted that there is no discontinuity in the experimental $B_{r2}(r)$ distribution at $r \sim 150$ mm, i.e. in the region of the profile discontinuity the measured B_{r2} is in agreement with theory for the average profile angle and not the detailed profile angle within the discontinuity. This supports the idea that the discontinuity is a wave superimposed on an otherwise steady profile.

Figure 12 shows magnetic probe oscillograms in the region of r^*. For $r > r^*$, e.g. $r = 85$ mm, the shock transition involves increases in both B_r and B_z, i.e. the characteristics of a pure oblique shock with positive tilt α. The decrease in B_z due to the rotational effects of the piston follows closely behind the shock for radii close to r^*. For $r \sim r^*$, e.g. $r = 78$ mm there is negligible change in B_z accompanying the B_r rise of the shock, i.e. demonstrating the presence of a pure switch-on shock.

5.2 Case (1): Shock-Intermediate Wave Model

The experimental $B_{r2}(r)$ distribution continues smoothly through the point of parallel propagation into the region $r < r^*$ where the profile tilt is negative. Thus for $r < r^*$ the transverse field component is not simply increased as is required for a pure oblique shock, e.g. as happens for $r > r^*$, but the sign is reversed. It is also clear that, if a sudden reversal in the direction of B_{r2} occurred at r^*, flux would not be conserved. We may however satisfy the experimental facts by invoking the presence of a large amplitude intermediate wave behind the shock in the region $r < r^*$, which rotates the transverse field component through 180°. This model is illustrated in Fig.13, using discontinuous transitions spatially close together so that they have the same angle α. At $r = r^*$ the shock is of the

switch-on type and because, as such $v_2 = c_{i2}$, there is no tendency for the intermediate wave to separate from the shock. For $r < r^*$ the oblique shock and intermediate wave should separate with a relative velocity given by

$$v_{x2} - B_{x2}/(\mu \rho_2)^{\frac{1}{2}} .$$

This is however small for small α and because of finite structure thickness no separation would be seen on the time scale of the experiment.

The transition through the combined oblique shock and intermediate wave may be expressed, in cylindrical coordinate notation, as

$$\delta B_r = (B_{y2} + B_{y1}) \cos \alpha$$
$$\delta B_z = - (B_{y2} + B_{y1}) \sin \alpha .$$

Thus, unlike a pure oblique shock, this combined structure involves a decrease in B_z. The oscillogram of Fig.12 at $r = 60$ mm is in agreement with this model; the shock jump in B_r is accompanied by a decrease in B_z. The situation is however complicated by this decrease merging into the larger B_z decrease occurring at the piston.

This shock-intermediate wave model is directly analogous to that proposed in Paper I (see Fig.15 of Paper I) where a 90° intermediate wave follows the shock in the oblique region adjacent to the point of parallel propagation, thus producing the B_θ component observed in the experiment.

5.3 Case (1): Shock Structure

The radial variation of the shock structure is illustrated in Fig.14. Curve "C" shows the position of peak $\dot{B}_r$ obtained by converting the best fit experimental curve of Fig.11(a) into a spatial profile. Positions of the other features are measured relative to 'C'.

One dimensional conservation and structure theory should be applicable to individual points along the profile because the radius of curvature of the profile is much larger than the shock thickness and the dominant J_θ current of the shock is unconnected along the profile.

Bickerton et al (1971) have computed theoretical oblique and switch-on shock structures using a two fluid model with classical transport coefficients. In a comparison of computed and experimental structure made in Paper I for the switch-on shock it was found that a resistivity $\eta = 20\,\eta_{class}$ was necessary in the computations to damp the precursor whistler structure sufficiently to agree with the experimental structure. Because the switch-on shock was was subcritical ($M_A = 1.3 < M_A^* \sim 1.5$) the computed structure was not strongly dependent on viscosity. It should be noted however, that the computations neglect thermal conductivity and shear viscosity both of which could be important in the switch-on shock. It is suggested in Paper I that the enhanced resistivity of the shock was possibly

due to excitation of the ion acoustic instability, the onset conditions of which, i.e. electron drift velocity $v_d >$ sound speed s and $T_e > T_i$ (Stringer (1964)), were probably satisfied although the former only marginally.

In the present case we compare computed structures with the experimental structures at the positions on the profile of Fig.14 indicated by the dashed lines. At position 'X' ($\alpha = 30^o$) a resistivity $\eta \sim 6\, \eta_{class}$ in the computed structure produces agreement with experiment whilst at position 'Y' ($\alpha = 0^o$) $\eta \sim 15\, \eta_{class}$ is necessary.

At 'Y' the peak current density $J_{\theta_{max}} \sim 4 \times 10^6$ A/m^2 is comparable with $J_{r_{max}}$ of Paper I at the switch-on shock and hence $v_d \sim 3 \times 10^4$ m/sec again is comparable with s and conditions are marginally appropriate for excitation of the ion acoustic instability.

At 'X' $J_{\theta_{max}}$ is lower by a factor of ~ 2 due to the smaller field transition and the broader structure, and hence the ion acoustic instability should not be excited. The cause of the enhanced resistivity is uncertain but the larger resistivity enhancement at 'Y', where J_{max} is larger, is consistent with the presence of some current driven instability.

5.4 Case (2): High M_A Switch-on Shock

Fig.15(a) shows the radial variation in arrival time of shock and piston at $z = 0.4$ m for Case (2). We note:

(i) The shock profile is smooth in the region $90 < r < 180$ mm but is highly tilted (up to $\sim 50^{\circ}$).

(ii) There is a discontinuity in the profile at $r \sim 85$ mm. For $r < 85$ mm the shock and piston structures overlap and the situation is unclear.

(iii) A large discontinuity occurs in the profile at $r \sim 180$ mm.

Thus we do not in this case have the situation of a smooth shock profile passing through a point of parallel propagation and no switch-on shock is observed.

Fig.15(b) shows a comparison between the experimental $B_{r2}(r)$ distribution and the theoretical distribtion for the best-fit experimental profile. The agreement is not good. Also shown on Fig.15(b) as the dashed curve, is the theoretical distribution for a profile shown on Fig.15(a) (dashed curve) which links the low radius part of the experimental profile to the region outside the discontinuity at $r \sim 180$ mm. Agreement in this case is good. A reasonable interpretation of this result is that earlier in the shock trajectory the experimental profile approximated to the dashed curve, but, probably due to an excessive piston tilt, the profile could not be maintained and it collapses to a larger tilt by means of a wave or discontinuity propagating

radially outwards along the profile. The process is probably happening on a smaller scale in Case (1) Fig.11(a).

5.5 Case (3): Gas Dynamic Shock

Fig.16(a) shows the radial variation in arrival time of shock and piston at $z = 0.4$ m for Case (3). The peak $\dot{B}_r$ profile is smooth and passes through a region of parallel propagation at $r \sim 90$ mm but for $r \leqslant 100$ mm the shock and piston are almost coincident and it is unclear whether the B_r rise is the true shock or merely the result of radial plasma motion from diamagnetic and centrifugal effects associated with the piston.

Fig.16(b) shows a comparison of the measured $B_{r2}(r)$ distribution with the theoretical distribution for the best-fit profile; the agreement in this case is good.

5.6 Discussion

In Case (1) a shock profile is produced with propagation angles ranging from $\alpha = 0^\circ$ to $\sim 35^\circ$. This therefore complements the experiment of Robson and Sheffield reviewed in section 1.2, where angles of $\alpha = 90^\circ$ to 40° were produced. The transition is shown to be that of a low M_A switch-on shock at the point of parallel propagation ($r = r^*$). In the region $r < r^*$ where the tilt angle is negative it is suggested that a large amplitude intermediate wave follows closely behind the oblique shock rotating the transverse field component through 180° to

produce the experimentally observed post-shock B_r component.

No such switch-on shock was produced in Case (2), where initial conditions were appropriate to the production of a high M_A switch-on shock ($M_A \sim 1.7$). In Paper I it also was only found possible to produce switch-on shocks with low M_A ($\leqslant 1.4$). It has been demonstrated theoretically by Woods (1971) that the switch-on shock should only be stable in the region $M_A < M_A^*$ ($M_A^* = 1.53$ for $\beta_1 = 0$). A simple argument, based on two fluid theory of low frequency dispersion curves, which arrives at the same result has been set out in Paper I.

In case (3) it was not possible to identify a separated gasdynamic shock. Although a magnetic probe should not register the arrival of such a shock, the adjacent oblique regions do involve magnetic field changes and would therefore be observable.

6. SUMMARY

For a wide range of initial parameters we have successfully launched a weakly curved shock profile, clearly separated from its driving piston, into a well diagnosed initial plasma. Propagation angles to the initial field range from $\alpha = 0^\circ$ to $\sim 40^\circ$. The profile is quasi-steady and propagates with approximately constant velocity. The radius of curvature of the profile is considerably larger

than the shock thickness thus making comparison with one-dimensional theory reasonable. A high degree of reproducibility has enabled shot by shot analysis of the flow with small magnetic probes.

Detailed results are presented for three sets of initial conditions where, for parallel propagation, we would expect a subcritical switch-on shock ($1 < M_A < M_A^*$), a supercritical switch-on shock ($M_A^* < M_A < \hat{M}_A$) and a gas-dynamic shock ($M_A > \hat{M}_A$). Parallel propagation in the sub-critical switch-on shock case only was obtained and agreement with conservation theory demonstrated. This supports the theoretical result of Woods (1971) who concludes that super-critical switch-on shocks should not be stable.

The experimental demonstration of the existence of a stable switch-on shock given in the present paper is considerably clearer than that given in Paper I where centrifugal effects and small shock profile radius of curvature severely complicated the flow pattern.

For radii inside the switch-on shock position, where a negative tilt occurs, the observed field transition requires the presence of a large amplitude intermediate wave immediately behind oblique shock.

Comparison between measured and computed oblique and switch-on shock structures, demonstrates the presence of

an enhanced resistivity. Conditions are not however appropriate for the excitation of the usual microinstabilities present in plasma shock waves.

ACKNOWLEDGEMENTS

The author is grateful to Dr J.W.M. Paul for many useful discussions and valuable suggestions, and to Dr R.J. Bickerton for his encouragement and support.

Thanks are due to Mr L.S. Holmes for his technical assistance.

REFERENCES

ANDERSON, J.E. 'M H D Shock Waves' M I T (1963).

BICKERTON, R.J., LENAMON, L. and MURPHY, R.V.W., J. Plasma Physics, 5, 177 (1971).

CRAIG, A.D. and PAUL, J.W.M., J. Plasma Physics, 9, 161 (1973).

KANTROWITZ, A. and PETSCHEK, H.E. In 'Plasma Physics in Theory and Applications', ed. Kunkel, W.B. (McGraw-Hill Book Company, Inc., N.Y. 1966).

KURTMULLAEV, R.Kh, MASALOV, V.L., MEKLER, K.I. and SEMENOV, V.H., Soviet Physics J E T P, 33, 216 (1971).

PAUL, J.W.M. 'Physics of Hot Plasmas', eds. Rye, B.J. and Taylor, J.C., Oliver and Boyd, (1970) p.302.

ROBSON, A.E. and SHEFFIELD, J., Third International Conference on Plasma Physics and Controlled Nuclear Fusion, Novosibirsk, (1968). Proc. I A E A, Vienna, 1969, vol.1, pp.119-128.

SHEFFIELD, J., DECKER, G., MacMAHON, A.B. and ROBSON, A.E. Fourth European Conference on Controlled Fusion and Plasma Physics, Rome, (1970) p.58.

STRINGER, T.E. Plasma Physics (J. of Nuclear Energy Pt C) 5, 89 (1963).

STRINGER, T.E., Plasma Physics (J. of Nuclear Energy Pt.C) 6, 267 (1964).

WATSON-MUNRO, C.N., CROSS, R.C. and JAMES, B.W., Third International Conference on Plasma Physics and Controlled Nuclear Fusion, Novosibirsk, (1968). Proc. I A E A, Vienna, 1969, vol.2, pp.195-207.

WOODS, L.C., J. Plasma Physics, 6, 615 (1971).

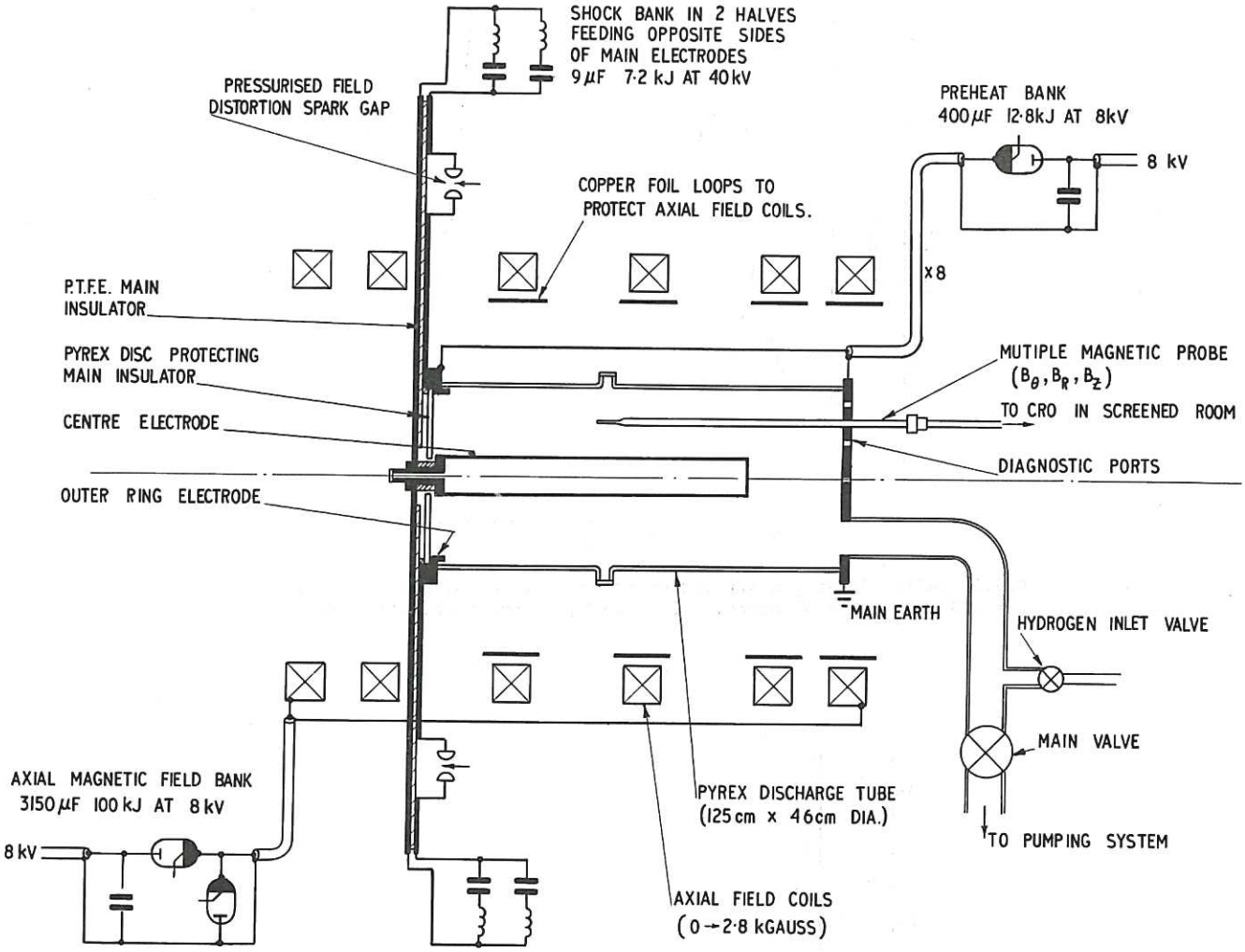

Fig.1 Schematic of the CHARYBDIS apparatus.
CLM-P364

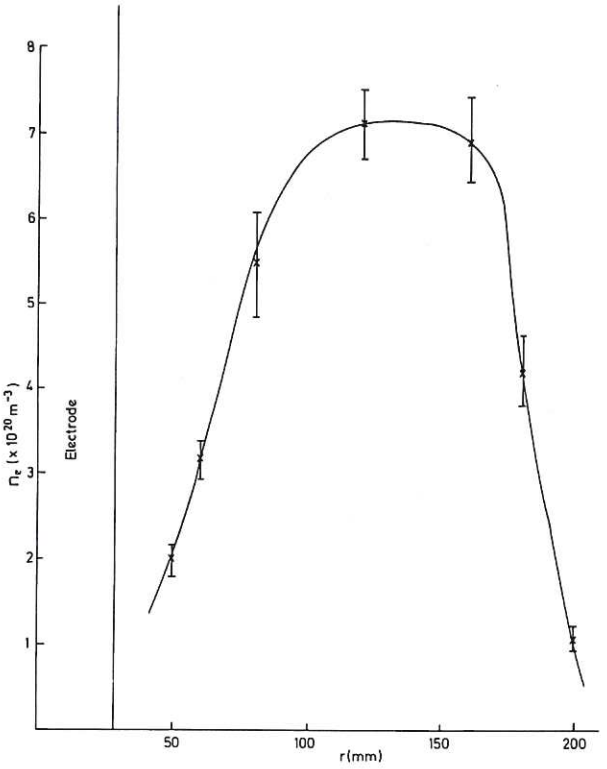

Fig.2 Radial density distribution of the initial plasma (z = 0.46 m, t = 300 μsec, p_1 = 40 mtorr, B_{z1} = 0.2 T, standard deviations).

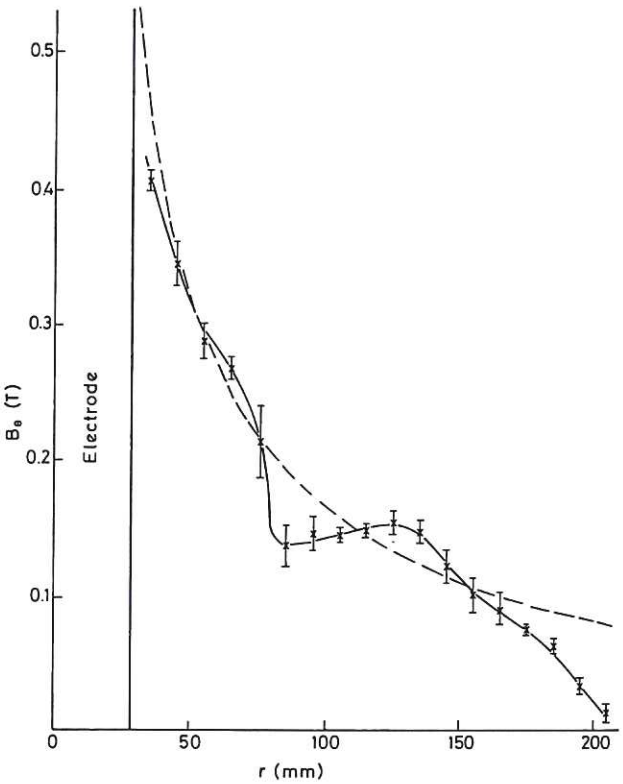

Fig.3 $B_\theta(r)$ distribution behind the main current front (z = 0.4 m, t = 4 μsec, p_1 = 20 mtorr, B_{z1} = 0.2 T, standard deviations).

CLM-P364

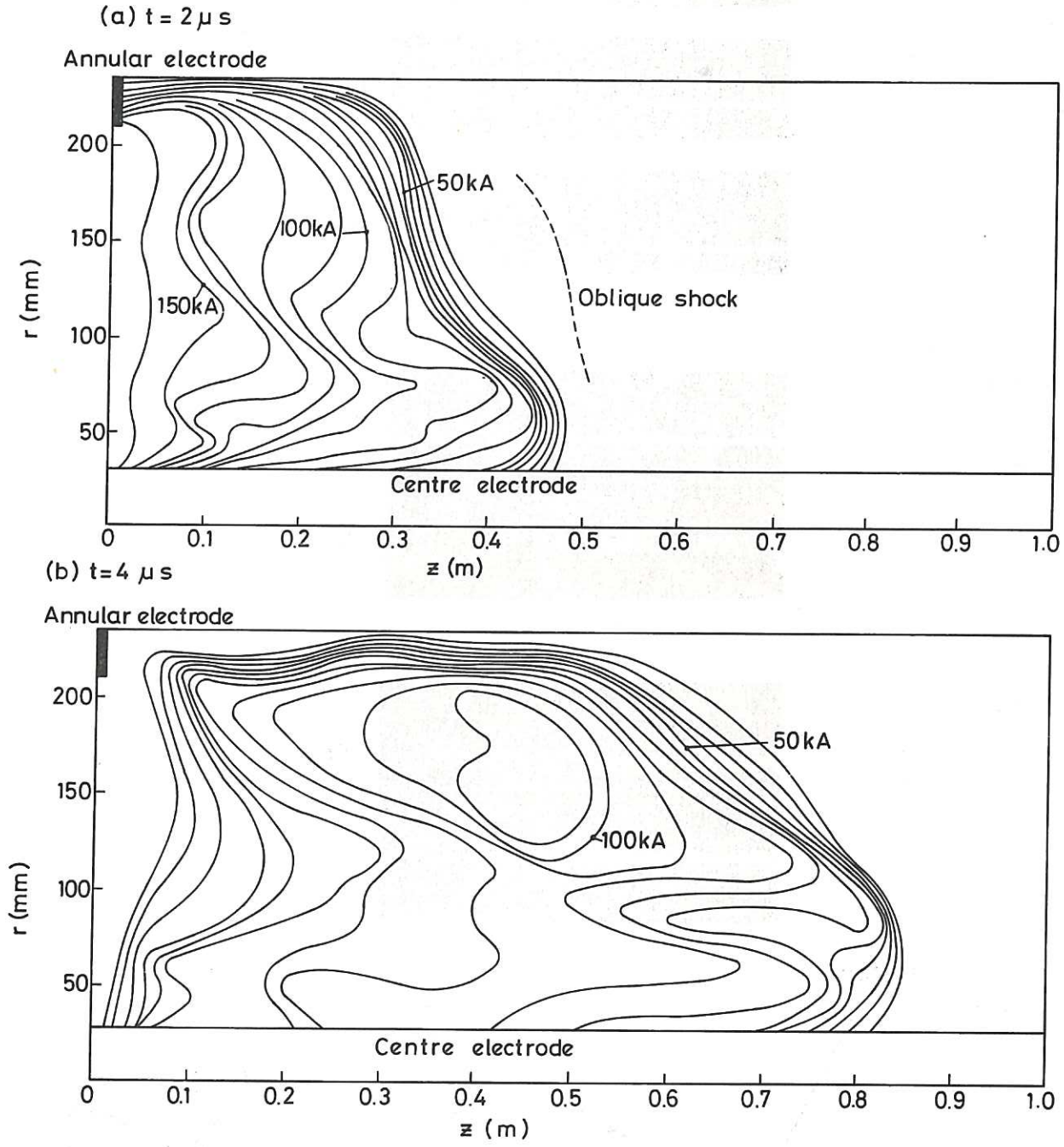

Fig.4 Current flow pattern in the rz plane (p_1 = 20 mtorr, B_{z1} = 0.2 T).
CLM-P364

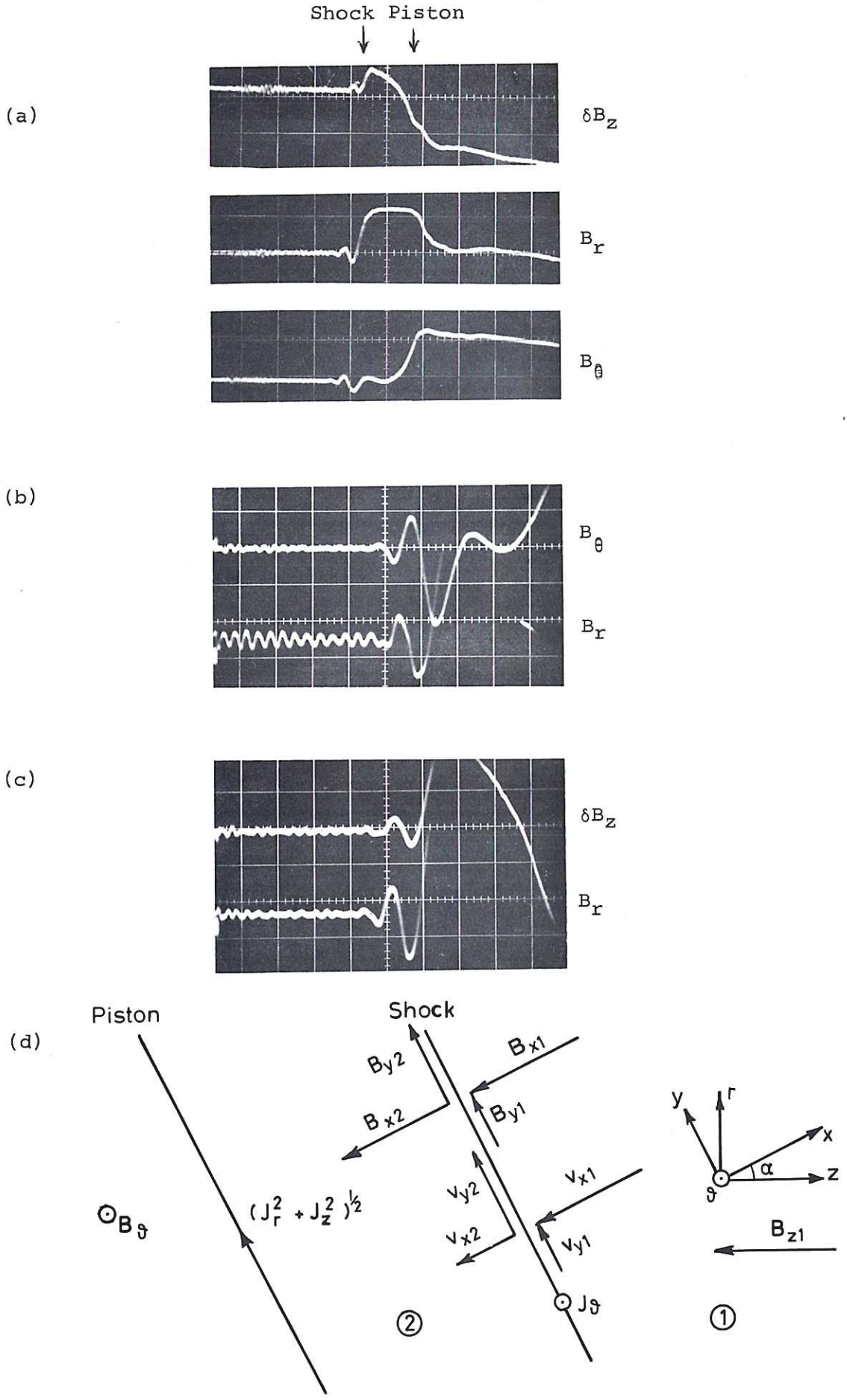

Fig.5 (a) Typical oscillograms showing the magnetic structure of the shock and piston (z = 0.4 m, r = 142.5 mm, p_1 = 20 mtorr, B_{z1} = 0.2T, 0.5 μsec/div, δB_z and B_r 0.056 T/div, B_θ 0.14 T/div). (b) and (c). Detail of precursor oscillation (0.2 μsec/div, 0.014 T/div). (d) Shock-piston model.

CLM-P364

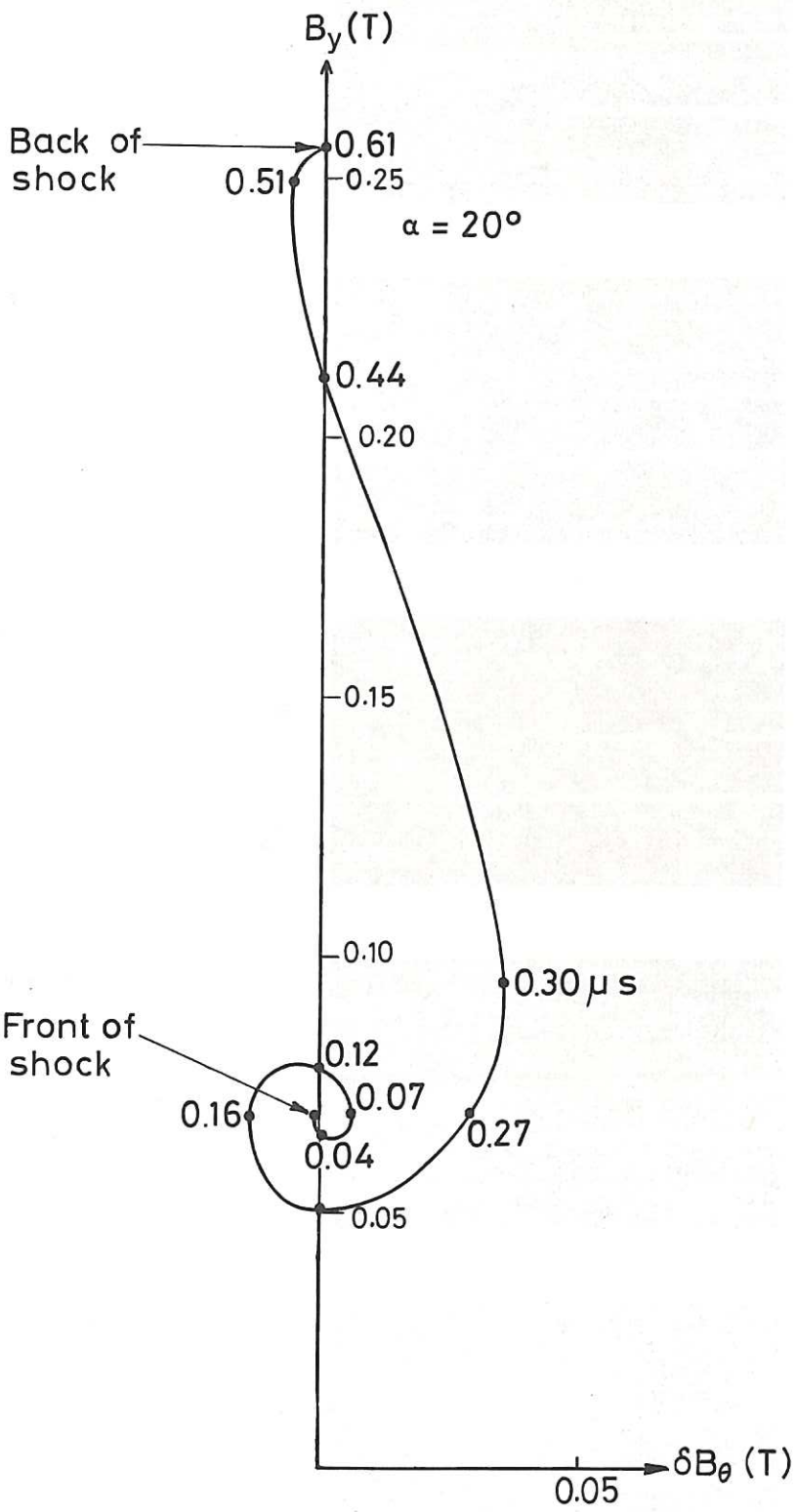

Fig.6 Rotation of the transverse field within the shock (p_1 = 20 mtorr, B_{z1} = 0.2 T).

CLM-P364

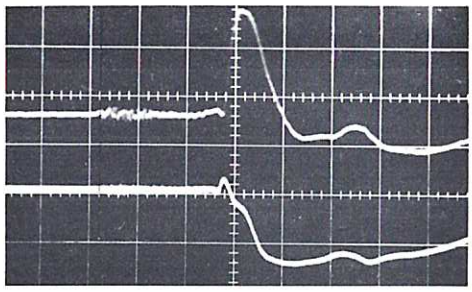

z = 0.2 m

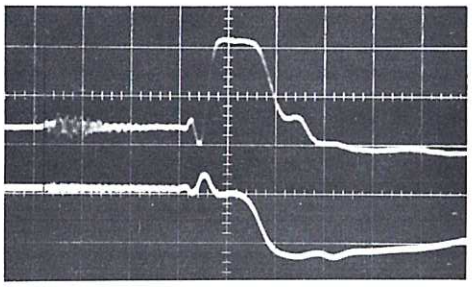

z = 0.3 m

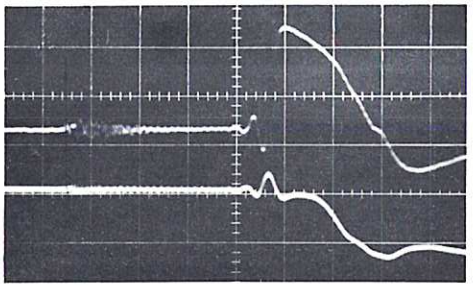

z = 0.4 m

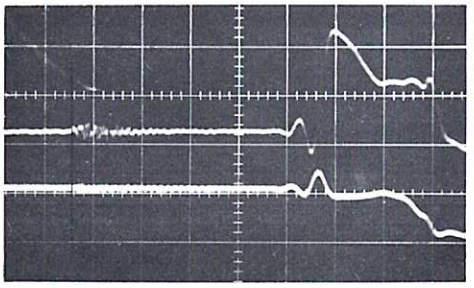

z = 0.5 m

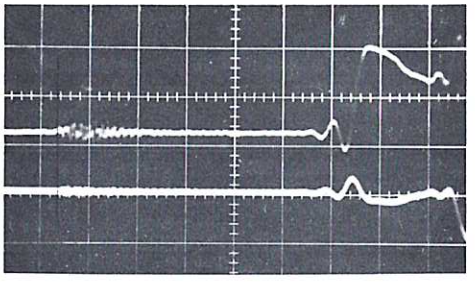

z = 0.6 m

Fig.7 Axial propagation and separation of shock and piston (r = 142.5 mm, p_1 = 20 mtorr, B_{z1} = 0.2T, 0.5 μsec/div, B_r 0.056 T/div, B_θ 0.14 T/div). CLM-P364

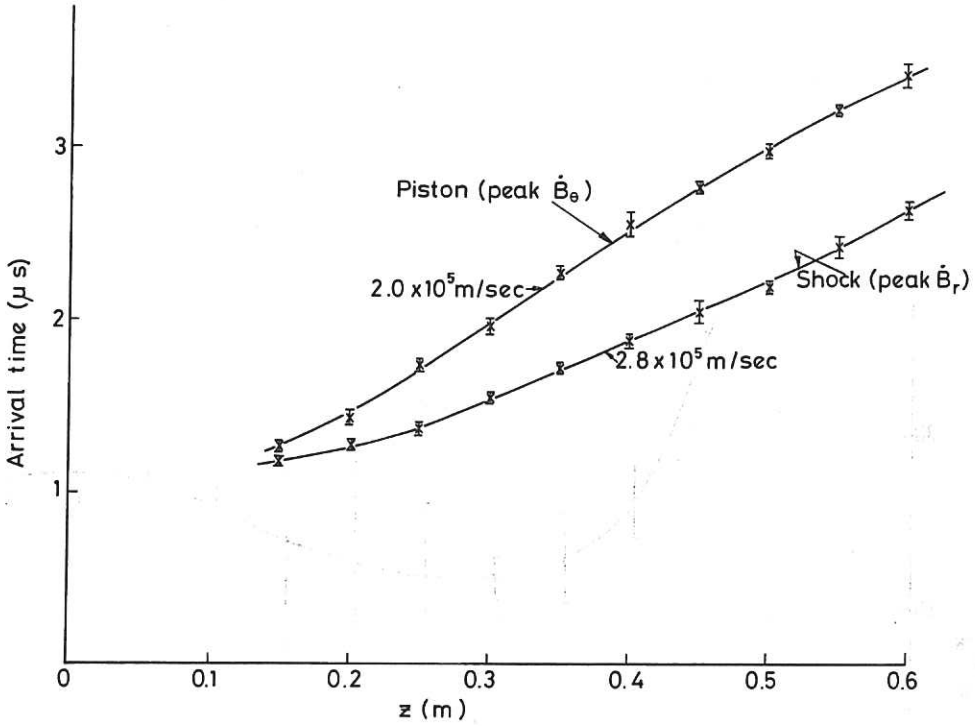

Fig.8 Axial propagation of shock and piston (r = 142.5 mm, p_1 = 20 mtorr, B_{z1} = 0.2 T, standard deviations).

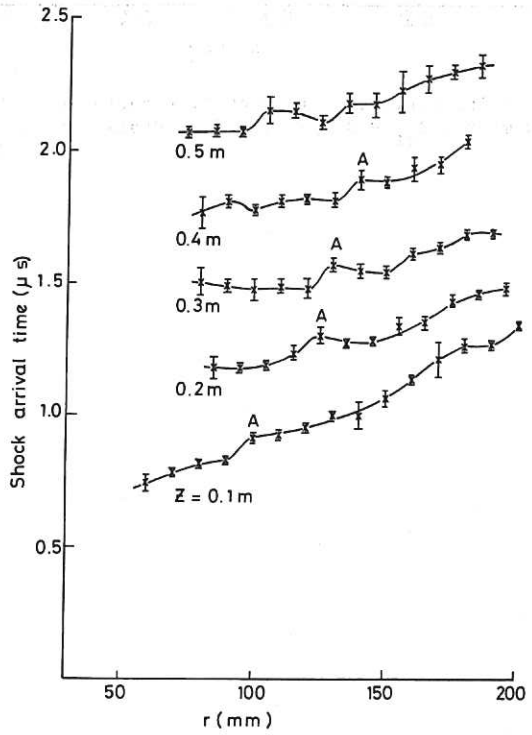

Fig.9 Radial variation in arrival time of shock at a series of axial positions (p_1 = 20 mtorr, B_{z1} = 0.2 T, standard deviations).

CLM-P364

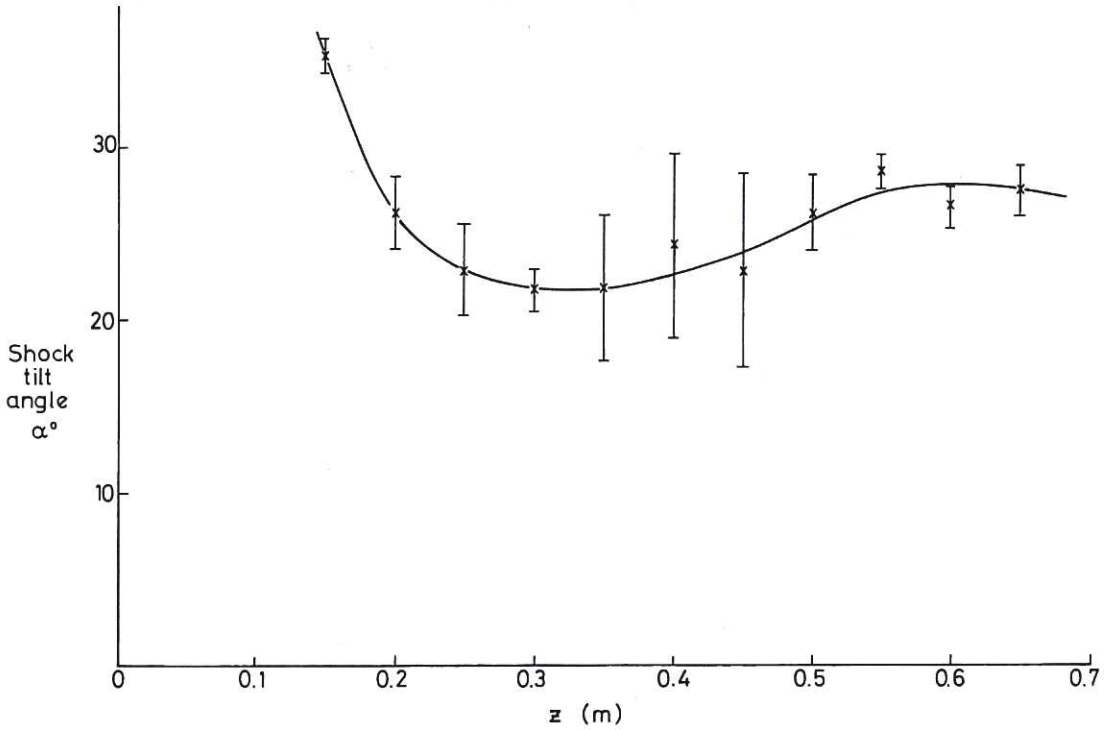

Fig.10 Axial variation of shock tilt angle (r = 142.5 mm, P_1 = 20 mtorr, B_{z1} = 0.2 T, standard deviations).

CLM-P364

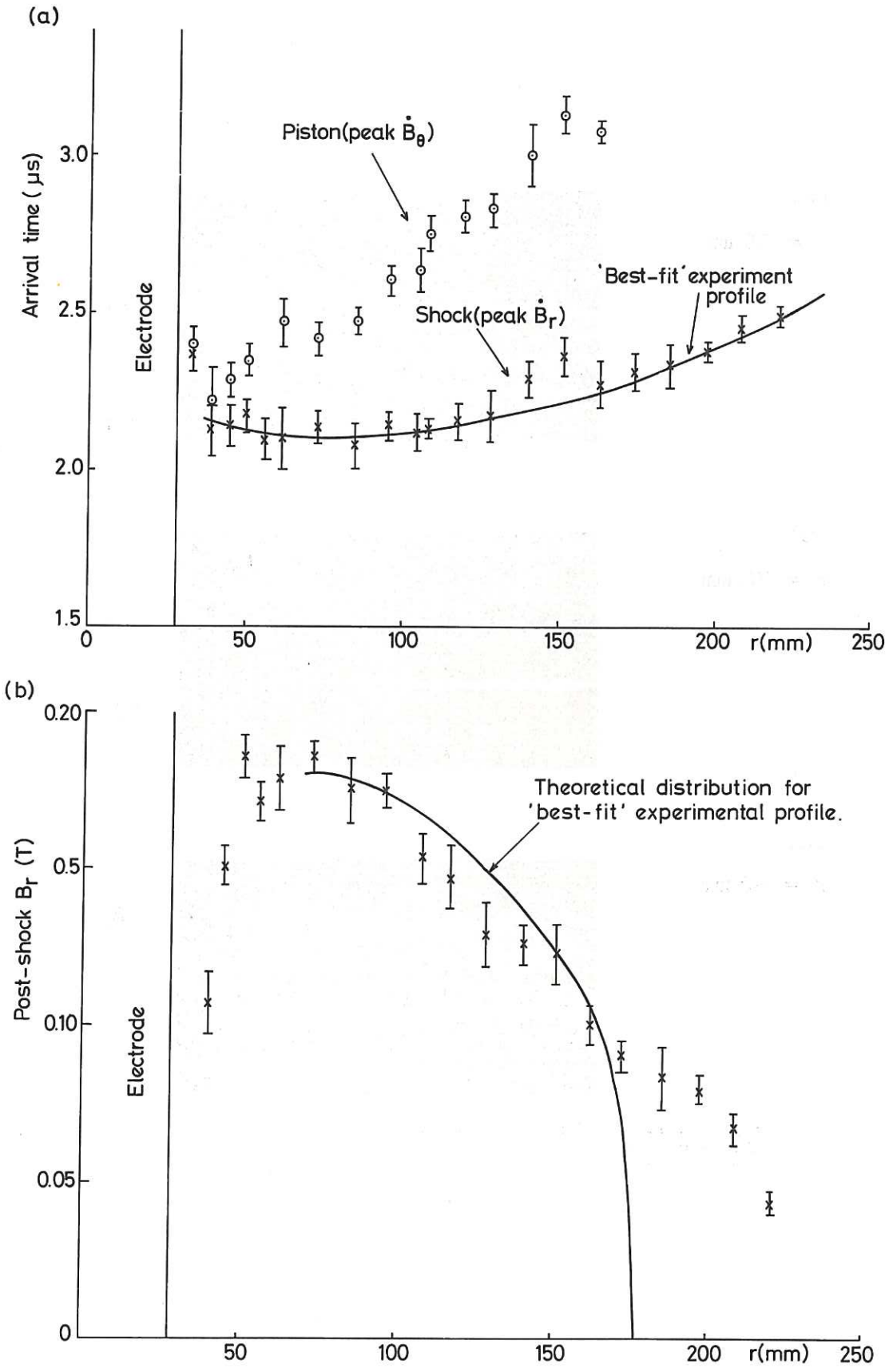

Fig.11 (a) Case (1): Radial variation of shock and piston arrival time (z = 0.4 m, standard deviations). (b) Case (1): Post-shock B_r versus radius (z = 0.4 m, standard deviations).

CLM-P364

(a)

r = 85 mm

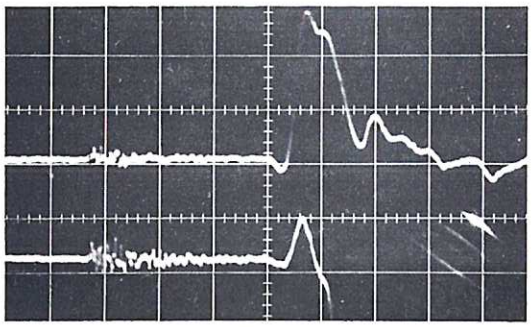

(b)

r = 78 mm

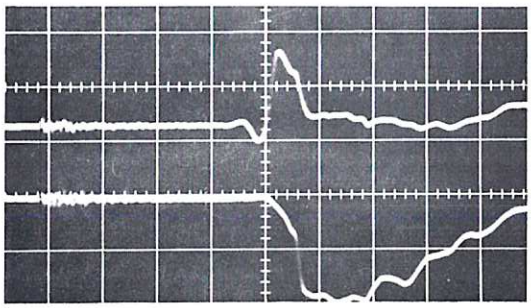

(c)

r = 62 mm

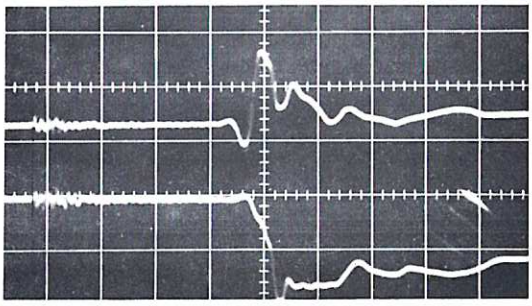

Fig.12 Case (1): Magnetic field structure in the region of the point of parallel propagation (z = 0.4 m, 0.5 μsec/div, r = 85 mm, 0.056 T/div, r = 78 and 60 mm, 0.14 T/div).

CLM-P364

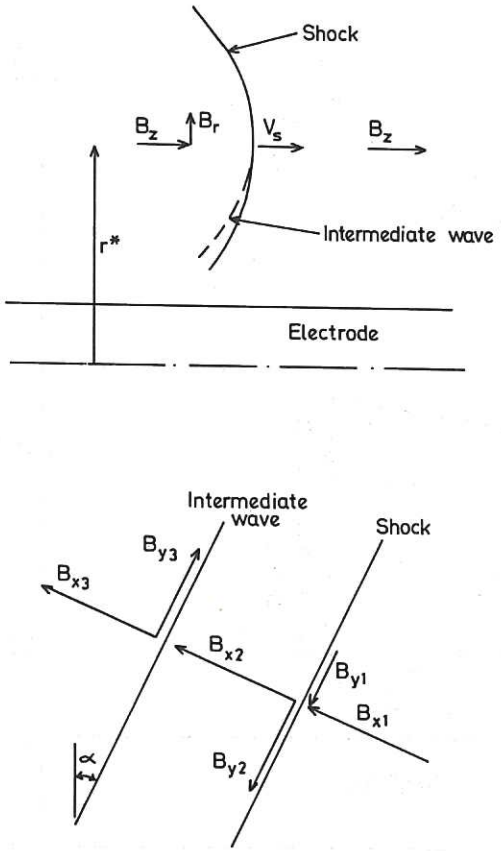

Fig.13 Shock-intermediate wave model.

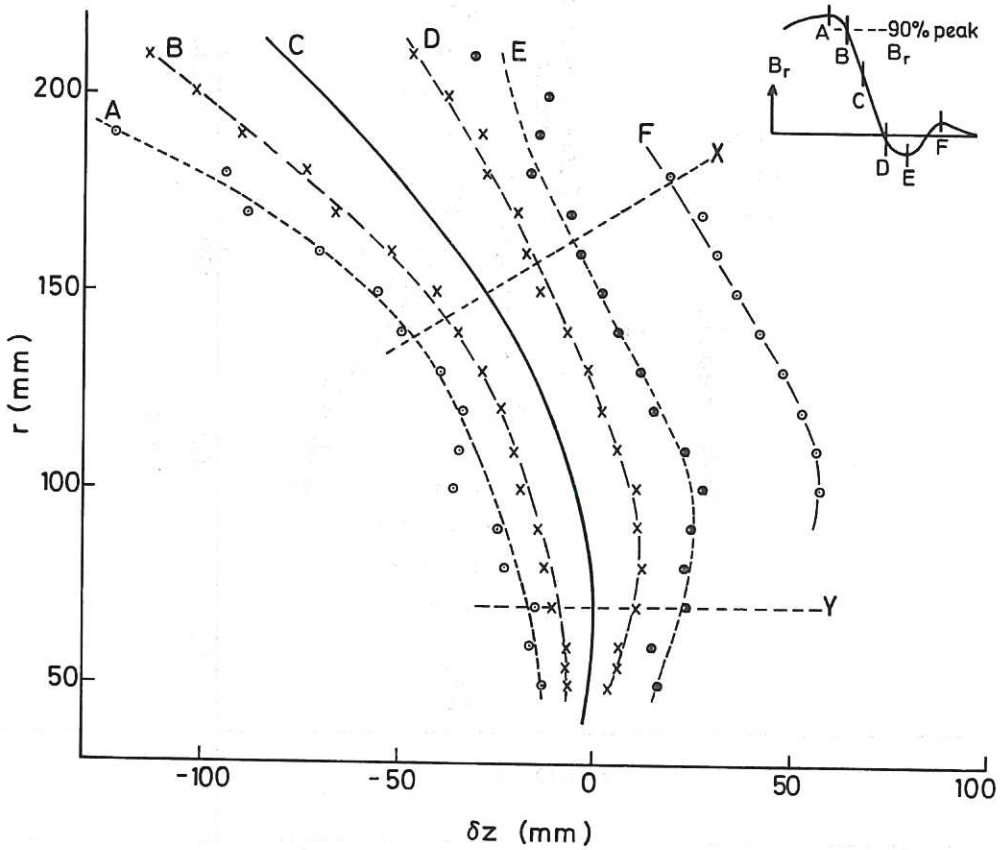

Fig.14 Case (1): Radial variation of shock structure (z = 0.4 m).
CLM-P364

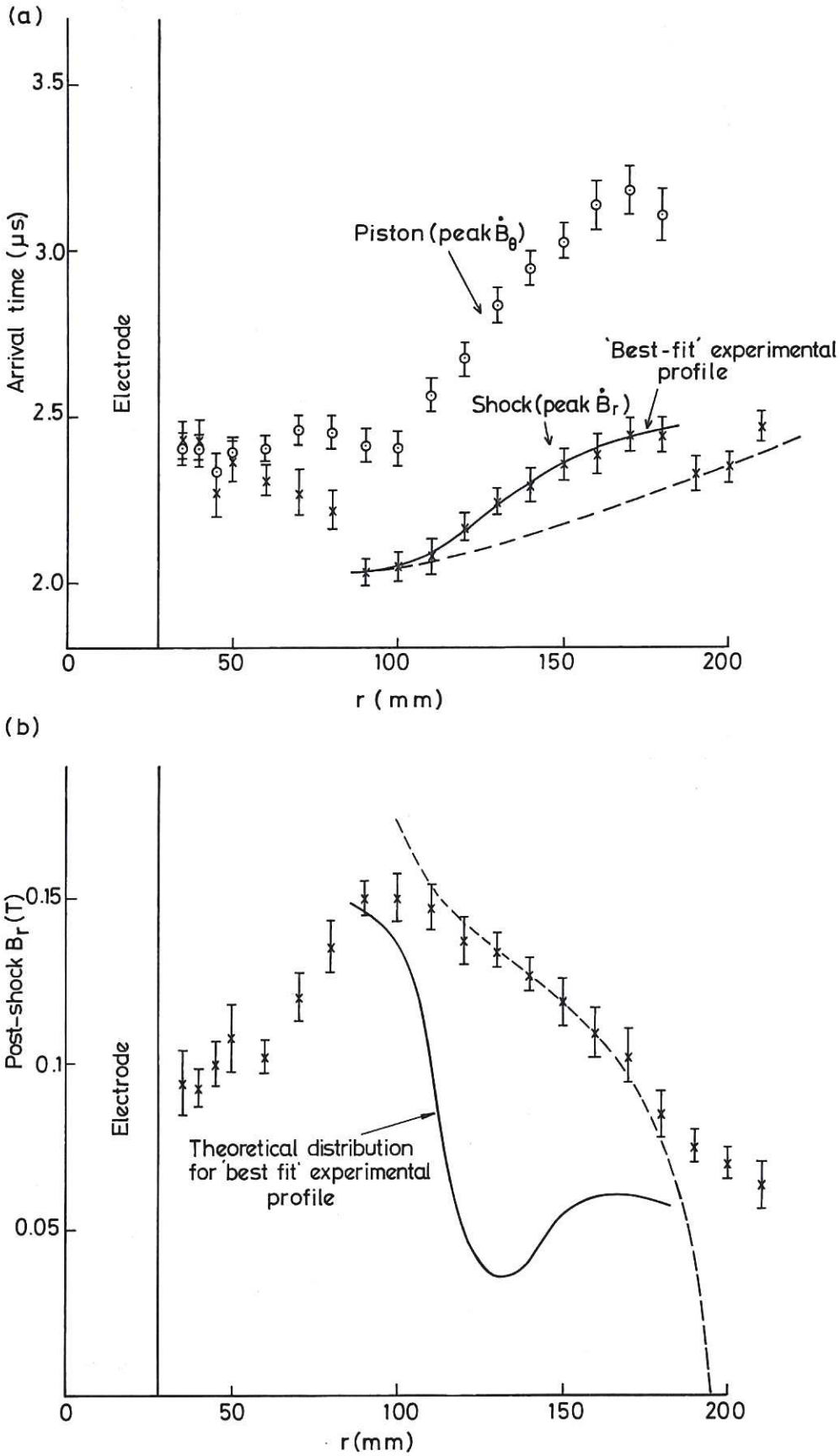

Fig.15 (a) Case (2): Radial variation of shock and piston arrival time (z = 0.4 m, standard deviations). (b) Case (2): Post-shock B_r versus radius (z = 0.4 m, standard deviations). CLM-P364

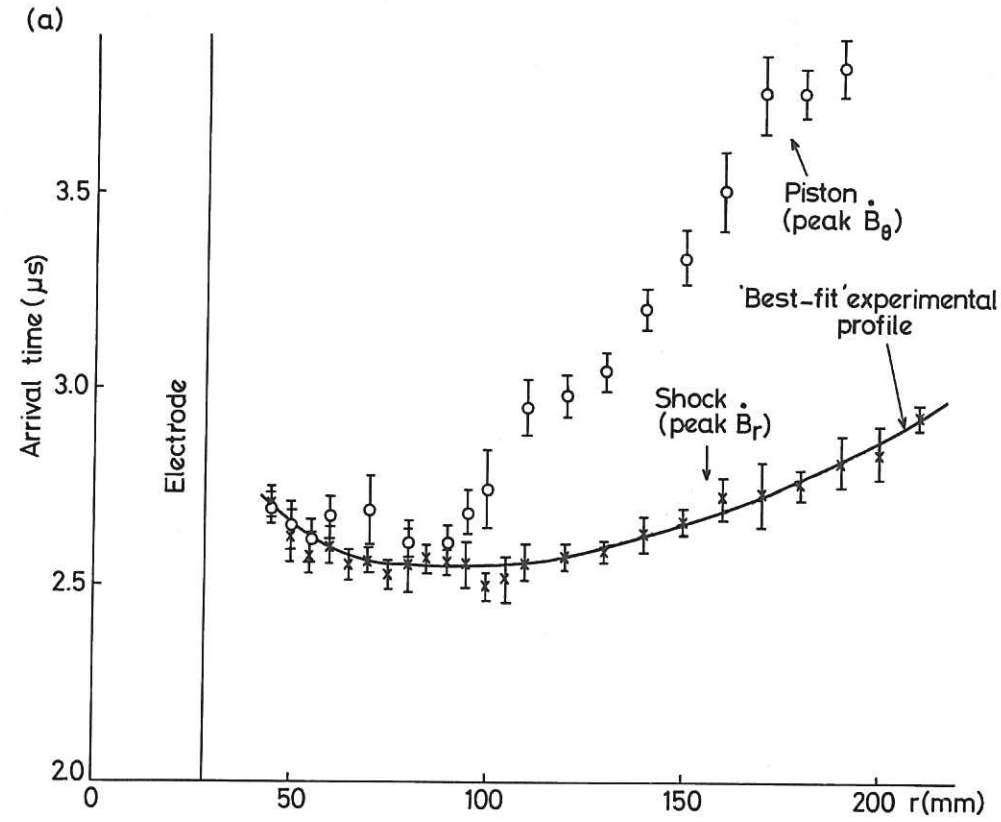

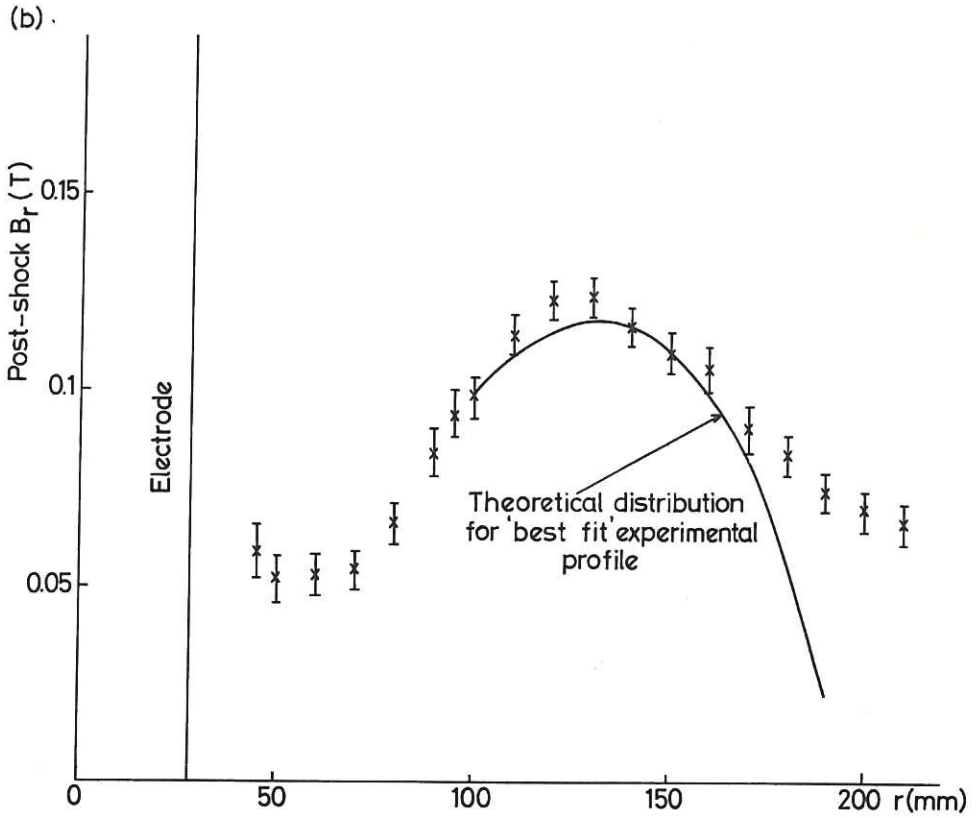

Fig.16 (a) Case (3): Radial variation of shock and piston arrival time (z = 0.4 m, standard deviations). (b) Case (3): Post-shock B_r versus radius (z = 0.4 m, standard deviations). CLM-P364